Supporting Information

Guanidinato Complexes of Iridium: Ligand-Donor Strength, O_2 Reactivity, and (Alkene)peroxoiridium(III) Intermediates

Matthew R. Kelley and Jan-Uwe Rohde*

Department of Chemistry, The University of Iowa, Iowa City, IA 52242

Contents | Page

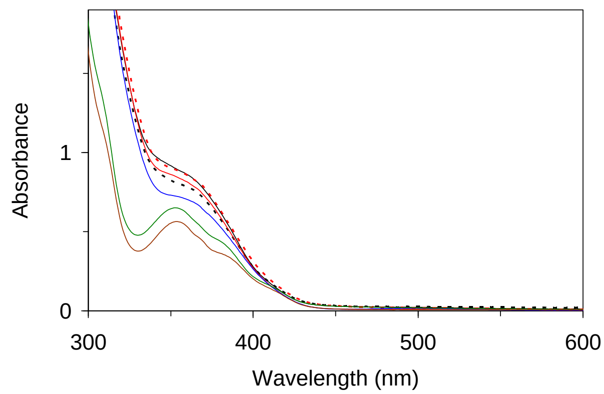

Figure S1. Electronic absorption spectra of 0.5 mM **2a**–**2g** in toluene (path length, 0.5 cm). Color key: **2a**, solid black line; **2b**, dashed black line; **2c**, solid red line; **2d**, dashed red line; **2e**, solid blue line; **2f**, solid green line; **2g**, solid brown line.

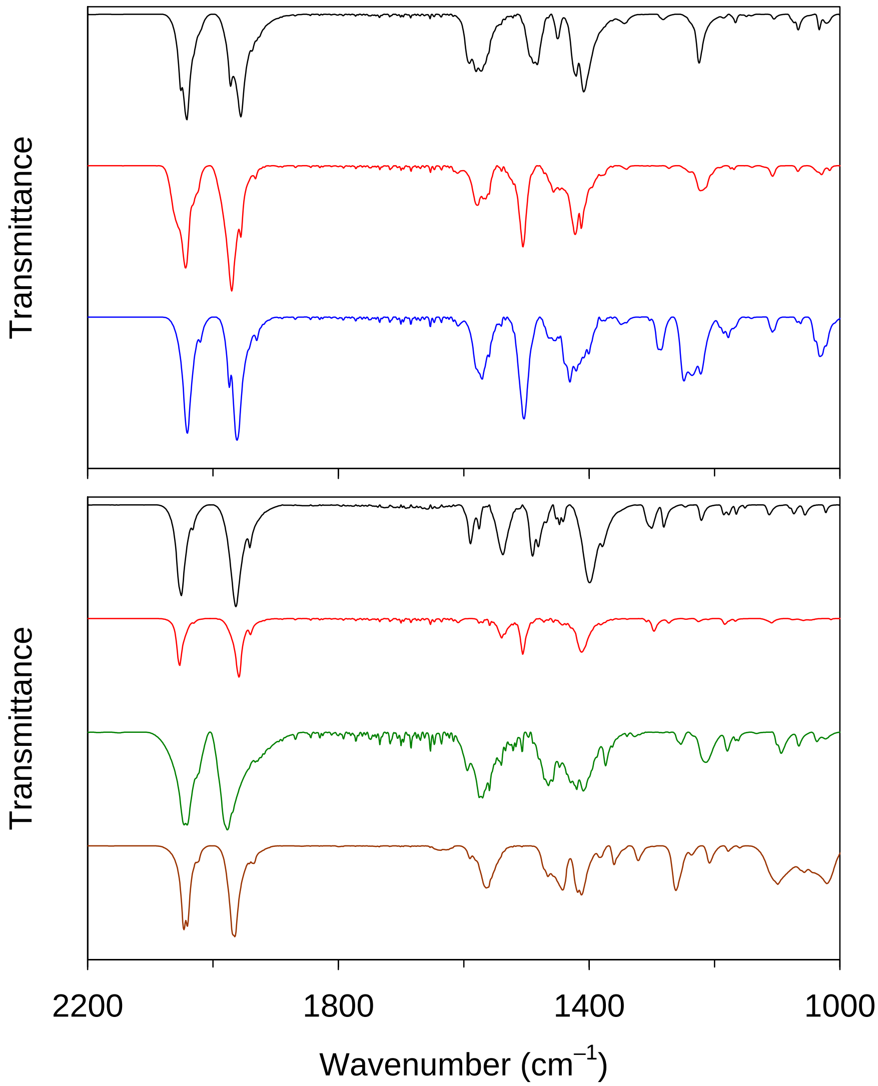

Figure S2. Solid-state IR spectra (KBr) of the dicarbonyl complexes **2a**–**2g**. Top: **2a** (—, black), **2c** (—, red), and **2e** (—, blue). Bottom: **2b** (—, black), **2d** (—, red), **2f** (—, green), and **2g** (—, brown).

Table S1. IR absorption bands of the dicarbonyl complexes **2a**–**2g** (2200–1000 cm^{-1}).[a]

Complex	ν_{CO} (cm^{-1})	ν (cm^{-1})			
2a	2051 (m), 2042 (s), 1972 (m), 1956 (s)	1592, 1580, 1572	1489, 1483	1450, 1421, 1409	1225
2b	2051 (s), 2033 (w), 1963 (s), 1941 (m)	1589, 1575, 1538	1490, 1481	1448, 1399, 1379	1300, 1281, 1221
2c	2058 (sh), 2044 (s), 1970 (s), 1956 (m)	1578, 1565	1506	1457, 1422, 1413	1222
2d	2053 (s), 1958 (s), 1940 (w)	1540	1506	1412	1297
2e	2041 (s), 2021 (w), 1974 (m), 1962 (s), 1930 (w)	1580 (sh), 1571	1504	1455, 1430, 1401	1285, 1249, 1236, 1222, 1178, 1107, 1032
2f	2047 (s), 2041 (s), 1977 (s)	1594, 1570	1465	1420, 1409, 1374	1254, 1214, 1180, 1094, 1066
2g	2046 (s), 2041 (s), 1966 (s)	1591, 1564	1467, 1442	1419, 1412, 1360	1322, 1262, 1208, 1099, 1021

[a] Solid state (KBr disk).

Table S2. Additional crystal and data collection parameters for [Ir{(4-MeC_6H_4)NC(NEt_2)N(4-MeC_6H_4)}(cod)], **1d**, and [Ir{PhNC(NEt_2)NPh}$(CO)_2$], **2b**.

	1d	**2b**
Crystal habit, color	prism, yellow	rod, colorless
Crystal size	0.27 x 0.17 x 0.16 mm^3	0.36 x 0.08 x 0.08 mm^3
F(000)	592	992
θ range for data collection	3.00 to 27.87°	3.32 to 27.87°
Limiting indices	$-12 \le h \le 12$, $-12 \le k \le 12$, $-17 \le l \le 17$	$-22 \le h \le 19$, $-22 \le k \le 22$, $-8 \le l \le 8$
Completeness to θ	99.4 % (θ = 27.87°)	99.8 % (θ = 27.87°)
Max. and min. transmission	0.4708 and 0.3160	0.5963 and 0.1812
Refinement method	Full-matrix least-squares on F^2	Full-matrix least-squares on F^2

Table S3. Selected interatomic distances (Å) for [Ir{(4-MeC_6H_4)NC(NEt_2)N(4-MeC_6H_4)}(cod)], **1d**, and [Ir{PhNC(NEt_2)NPh}$(CO)_2$], **2b**.[a]

1d		**2b**	
Ir–N1	2.078(2)	Ir–N1	2.069(6)
Ir–N2	2.087(2)		
Ir–C20	2.115(3)	Ir–C10	1.832(9)
Ir–C21	2.107(3)		
Ir–C24	2.111(3)		
Ir–C25	2.104(3)		
N1–C1	1.347(4)	N1–C1	1.359(8)
N1–C2	1.412(4)	N1–C2	1.419(9)
N2–C1	1.350(4)		
N2–C9	1.411(4)		
N3–C1	1.359(4)	N2–C1	1.338(11)
N3–C16	1.457(4)	N2–C8	1.480(7)
N3–C18	1.472(4)		
C20–C21	1.417(5)	C10–O	1.171(11)
C24–C25	1.419(5)		

[a] Numbers in parentheses are standard uncertainties in the last significant figures. Atoms are labeled as indicated in Figures 2 and 3.

Table S4. Selected angles (°) for [Ir{(4-MeC_6H_4)NC(NEt_2)N(4-MeC_6H_4)}(cod)], **1d**, and [Ir{PhNC(NEt_2)NPh}$(CO)_2$], **2b**.[a]

1d		**2b**	
N1–Ir–N2	63.76(9)	N1–Ir–N1#1	63.8(3)
N1–Ir–C20	104.93(11)	C10–Ir–N1	103.9(3)
N1–Ir–C21	101.46(11)	C10#1–Ir–N1	167.5(3)
N1–Ir–C24	159.33(13)		
N1–Ir–C25	155.22(12)		
N2–Ir–C24	105.58(11)		
N2–Ir–C25	101.77(12)		
N2–Ir–C20	158.32(12)		
N2–Ir–C21	155.78(12)		
C21–Ir–C20	39.21(13)	C10#1–Ir–C10	88.5(5)
C25–Ir–C24	39.35(13)		
C24–Ir–C20	90.50(13)		
C25–Ir–C20	81.34(14)		
C21–Ir–C24	81.71(13)		
C25–Ir–C21	98.25(13)		
C1–N1–C2	125.7(2)	C1–N1–C2	126.0(6)
C1–N1–Ir	93.71(17)	C1–N1–Ir	94.5(4)
C2–N1–Ir	133.00(18)	C2–N1–Ir	133.7(5)
C1–N2–C9	126.4(2)		
C1–N2–Ir	93.23(17)		
C9–N2–Ir	132.86(18)		
C1–N3–C16	121.4(3)	C1–N2–C8	120.9(4)
C1–N3–C18	121.0(2)		
C16–N3–C18	117.5(3)	C8#1–N2–C8	118.2(7)
N1–C1–N2	109.3(2)	N1#1–C1–N1	107.2(8)
N1–C1–N3	125.4(2)	N2–C1–N1	126.4(4)
N2–C1–N3	125.3(3)		

[a] Numbers in parentheses are standard uncertainties in the last significant figures. Atoms are labeled as indicated in Figures 2 and 3. Symmetry operation: #1, –y+3/2, –x+3/2, –z+3/2.

Table S5. Selected dihedral angles (°) for [Ir{(4-MeC_6H_4)NC(NEt_2)N(4-MeC_6H_4)}(cod)], **1d**, and [Ir{PhNC(NEt_2)NPh}$(CO)_2$], **2b**.[a]

1d		**2b**	
N1–C1–N2 / N1–Ir–N2	1.6(3)	N1–C1–N1#1 / N1–Ir–N1#1	0
N1–Ir–N2 / C20–Ir–C21	84.9(2)		
N1–Ir–N2 / C24–Ir–C25	84.7(2)		
C20–Ir–C21 / C24–Ir–C25	87.1(2)		
C16–N3–C18 / N1–C1–N2	33.9(2)	C8–N2–C8#1 / N1–C1–N1#1	39.6(6)
(N1,C1,N2,N3) / (C2→C7)[b]	48.0(1)	(N1,C1,N1#1,N2) / (C2→C7)[b]	44.7(3)
(N1,C1,N2,N3) / (C9→C14)[b]	46.1(1)		

[a] Numbers in parentheses are standard uncertainties in the last significant figures. Atoms are labeled as indicated in Figures 2 and 3. Symmetry operation: #1, –y+3/2, –x+3/2, –z+3/2. [b] Angle between the least-squares planes of the guanidinate atoms (*e.g.*, N1, C1, N2, and N3) and the aryl ring atoms (*e.g.*, C2, C3, C4, C5, C6, and C7).

Determination of the Self-Diffusion Coefficient of 2a

Diffusion ^{1}H NMR experiments to determine the D value of **2a** were conducted in triplicate, and, for each experiment, data of two suitable peaks were averaged. The average D value from three measurements was $(9.6 \pm 0.2) \cdot 10^{-10}$ $m^2 \cdot s^{-1}$ (ca. 17 mM **2a** in benzene-d_6, 400 MHz, 25 °C). Shown below are representative results for the NMe_2 resonance signal of **2a**. The plot in Figure S3 confirms the expected linear relationship between $\ln(I/I_0)$ and G^2.

```
SIMFIT RESULTS for 2a
==============

INTENSITY fit : Diffusion : Variable Gradient :
I=I[0]*exp(-D*SQR(2*PI*gamma*Gi*LD)*(BD-LD/3)*1e4)
16 points for Peak 4,  NMe2 resonance signal
Converged after 28 iterations!

Results     Comp. 1
I[0]           =  9.951e-001
Diff Con.      =  9.710e-010 m2/s
Gamma          =  4.258e+003 Hz/G
Little Delta   =      4.600m
Big Delta      =     26.950m

RSS   =   1.176e-004
SD    =   2.711e-003

Point     Gradient       Expt          Calc       Difference
    1   6.740e-001    1.000e+000    9.934e-001    -6.558e-003
    2   2.765e+000    9.693e-001    9.671e-001    -2.219e-003
    3   4.855e+000    9.091e-001    9.112e-001    2.114e-003
    4   6.945e+000    8.282e-001    8.310e-001    2.749e-003
    5   9.036e+000    7.296e-001    7.334e-001    3.860e-003
    6   1.113e+001    6.235e-001    6.266e-001    3.050e-003
    7   1.322e+001    5.156e-001    5.180e-001    2.365e-003
    8   1.531e+001    4.142e-001    4.146e-001    3.901e-004
    9   1.740e+001    3.217e-001    3.211e-001    -6.007e-004
   10   1.949e+001    2.429e-001    2.407e-001    -2.192e-003
   11   2.158e+001    1.767e-001    1.746e-001    -2.092e-003
   12   2.367e+001    1.249e-001    1.226e-001    -2.219e-003
   13   2.576e+001    8.519e-002    8.335e-002    -1.840e-003
   14   2.785e+001    5.695e-002    5.483e-002    -2.119e-003
   15   2.994e+001    3.680e-002    3.491e-002    -1.893e-003
   16   3.203e+001    2.283e-002    2.151e-002    -1.313e-003
============================================================
```

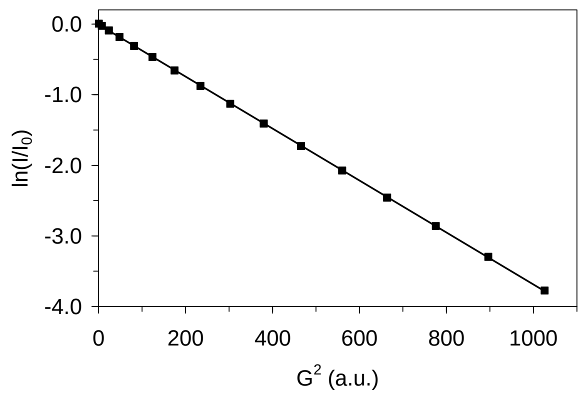

Figure S3. Plot of the natural logarithm of the intensity quotient, ln(I/I_0), as a function of the square of the gradient strength, G^2, for the NMe_2 resonance signal of **2a** in benzene-d_6 (ca. 17 mM, 400 MHz, 25 °C; R^2 = 0.99997).

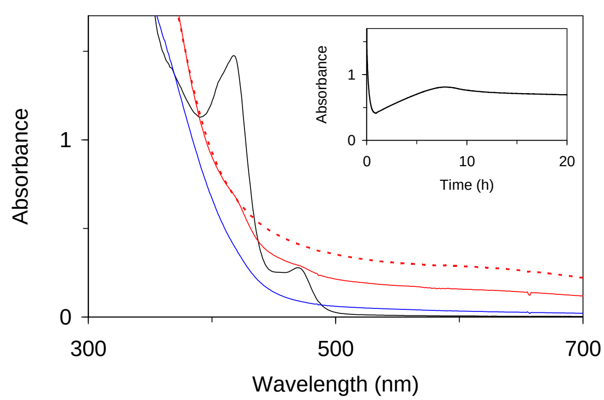

Figure S4. Electronic absorption spectra of 2 mM **1a** in toluene at 20 °C (solid black line), **3a** generated from the reaction of **1a** with O_2 (solid blue line; t = 1 h), and the solution after decay of **3a** under Ar (solid red line; t = 19 h; path length, 0.5 cm). Also shown is the spectrum of a solution obtained from decay of **3a** in toluene under O_2 at 20 °C (20 h after addition of O_2 to **1a**; dashed red line). Inset: Time course of the reaction of **1a** in toluene with O_2 at 20 °C and subsequent decay of **3a** under Ar (λ = 417 nm).

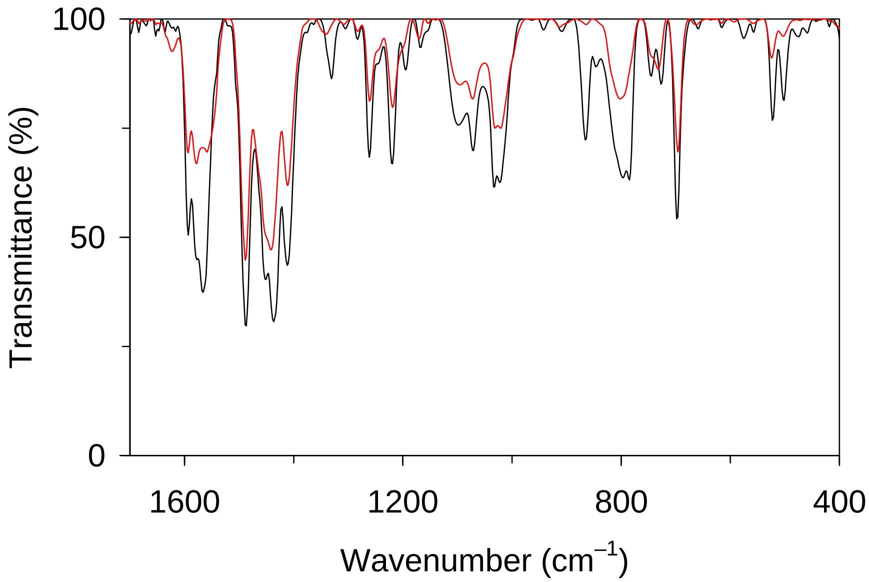

Figure S5. Solid-state IR spectra (KBr) of **3a** (—, black) and its decay products (—, red).

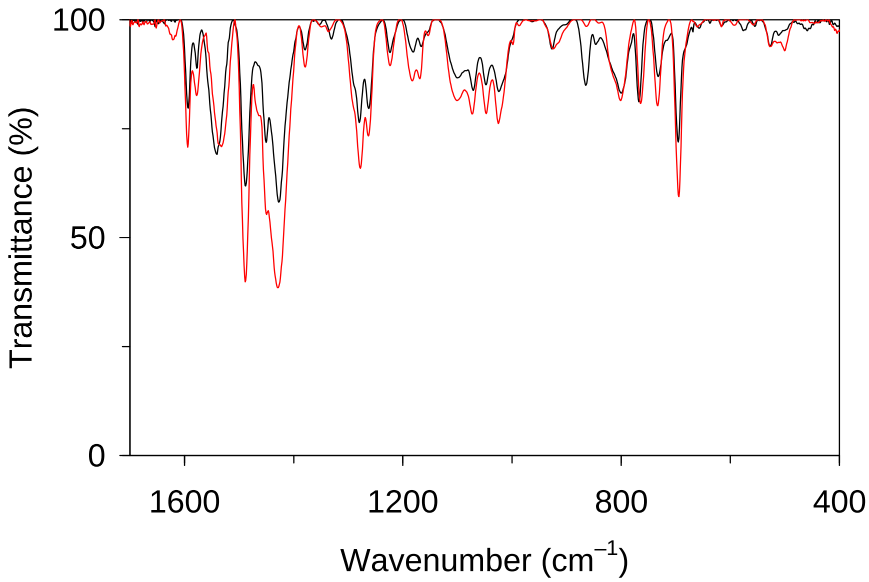

Figure S6. Solid-state IR spectra (KBr) of **3b** (—, black) and its decay products (—, red).

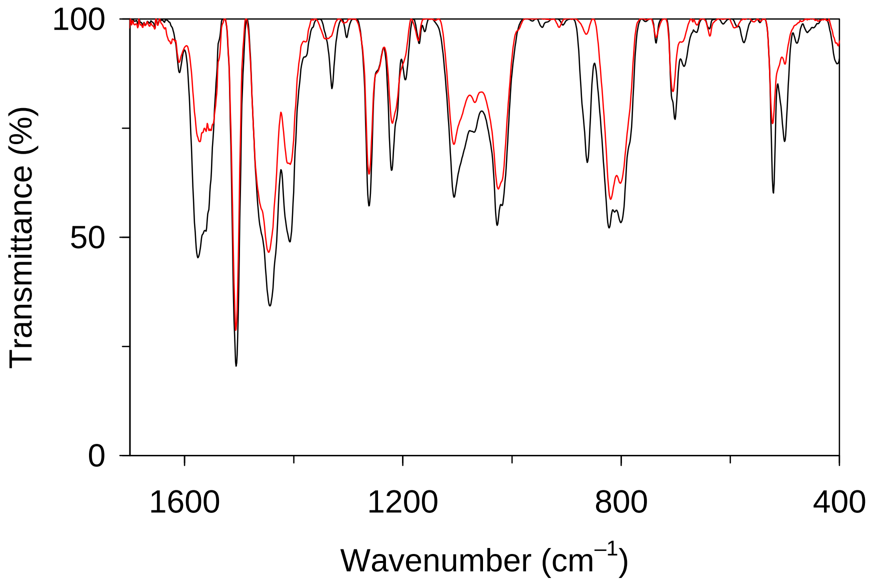

Figure S7. Solid-state IR spectra (KBr) of **3c** (—, black) and its decay products (—, red).

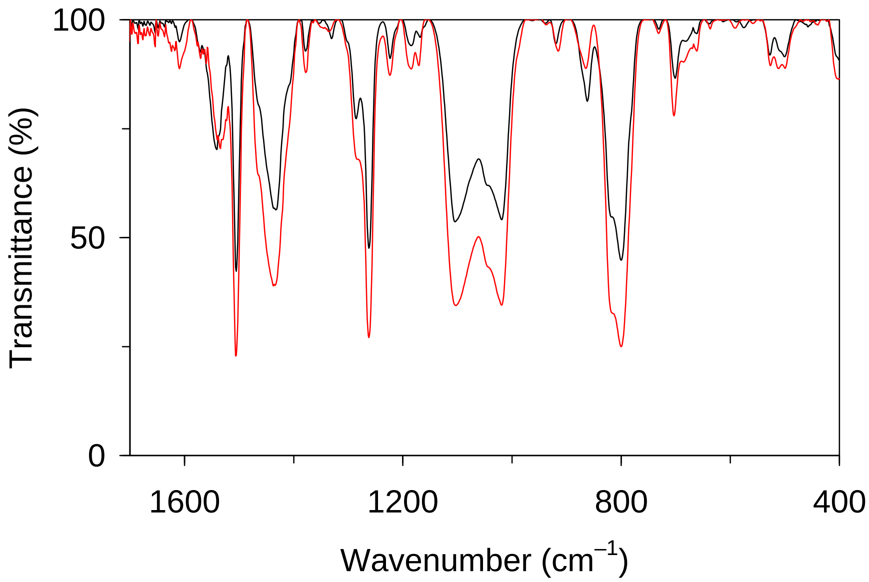

Figure S8. Solid-state IR spectra (KBr) of **3d** (—, black) and its decay products (—, red).

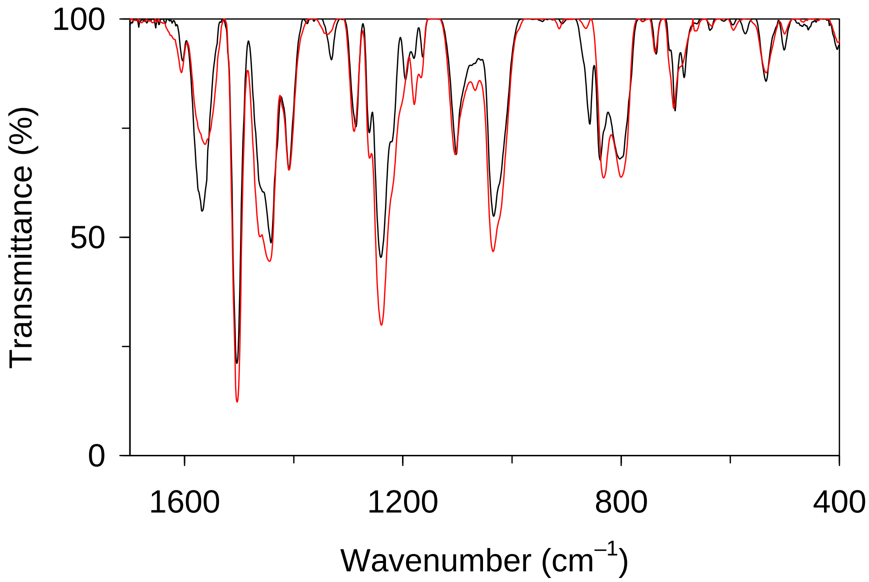

Figure S9. Solid-state IR spectra (KBr) of **3e** (—, black) and its decay products (—, red).

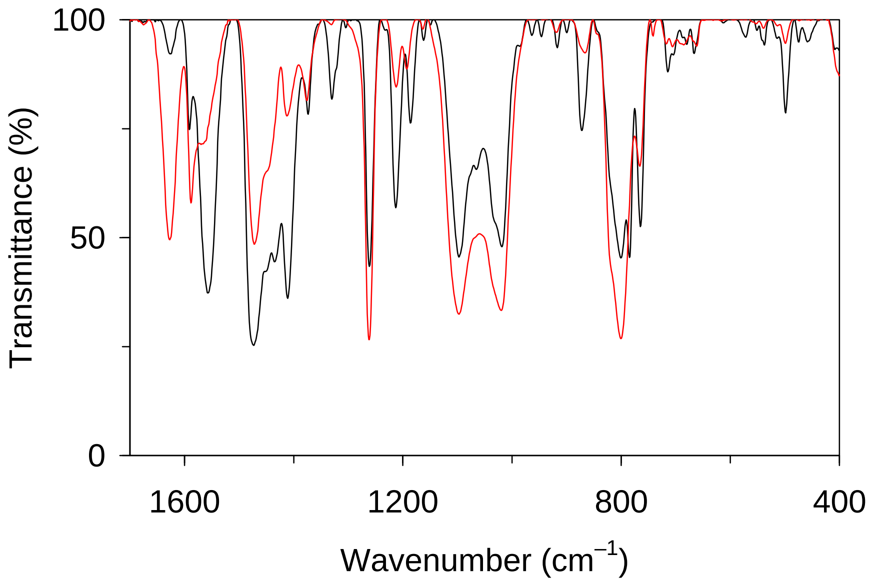

Figure S10. Solid-state IR spectra (KBr) of **3f** (—, black) and its decay products (—, red).

Table S6. IR absorption bands of the (alkene)peroxo complexes **3a**–**3f** (1700–1200 cm^{-1}).[a]

Complex	ν (cm^{-1})			
3a	1593, 1577 (sh), 1567	1488	1452, 1437, 1411	1331, 1261, 1220, 1195
3b	1593, 1577, 1541	1488	1450, 1427	1280, 1263, 1224
3c	1609, 1576, 1561 (sh)	1505	1444, 1407	1330, 1262, 1221, 1195
3d	1541	1505	1433	1286, 1262, 1223
3e	1603, 1568	1504	1461 (sh), 1442, 1409	1331, 1286, 1261, 1240, 1221 (sh), 1195
3f	1626, 1591, 1558	1473	1435, 1411, 1374	1330, 1261, 1213, 1186

[a] Solid state (KBr disk).

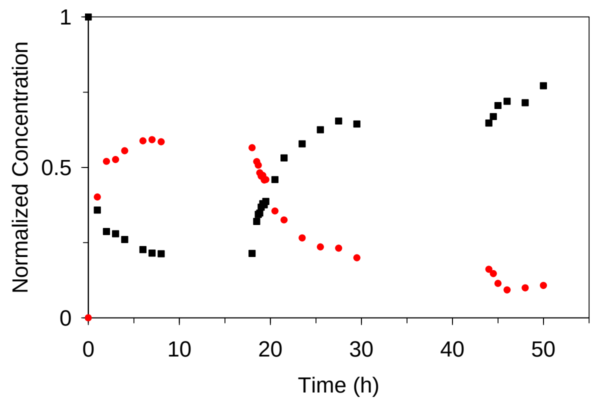

Figure S11. Time course (^{1}H NMR, 300 MHz) of the reaction of 18 mM **1f** (black squares) in benzene-d_6 with O_2 at 20 °C, producing **3f** (red circles), and regeneration of **1f**. To initiate the regeneration of **1f**, the solution was purged with Ar for 5 min after 18 and 44 h. Concentrations were determined using 1,2-dichloroethane as an internal standard and plotted relative to the initial concentration of **1f**.